A Comparative Study of Two Fault-Tolerant Dual-Motor Drive Topologies Under Short-Circuit Inverter Switch Fault

Tiago José dos Santos Moraes[1], Ngac Ky Nguyen[1], Fabien Meinguet[2], Eric Semail[1]
[1]Electrical Engineering and Power Laboratory of Lille (L2EP)
Arts et Métiers ParisTech
Lille, France
[2]Thales Alenia Space
Charleroi, Belgium
E-mail.[1]{tiago.dossantosmoraes ;ngacky.nguyen ; eric.semail}@ensam.eu
[2]fabien.meinguet@thalesaleniaspace.com

***Abstract*—This paper analyzes two dual-motor fault-tolerant topologies for aerospace thruster application. The first structure supplies independently both machines while the second one connects them in series for reducing the number of transistors and offering a capability of energy management between the sources. Inverter short-circuit fault is considered. Based on the peak-currents obtained in simulation in degraded mode without reconfiguration and with two different reconfiguration strategies, the two proposed topologies can be compared in economic and technical aspects.**

***Keywords*—series connected; multiphase machines; open-winding; fault-tolerance; reconfiguration; short-circuit fault; TVC system; dual-drives; dual-motor.**

I. INTRODUCTION

The application of the system analyzed in this paper is an aerospace Thrust Vector Control (TVC) system which needs to use simultaneously two electrical drives in order to properly control the direction of the thruster (see Fig. 1). For most of aerospace applications, fault-tolerance capability is highly required [1]-[3]. Fault-tolerance is achieved by supplementary Degrees of Freedoms (DoF) which ensure an acceptable operating system. For an inverter-machine drive, supplementary DoF can be presented in the form of supplementary inverter legs and/or multiphase machines [2]-[6].

In the present paper, fault-tolerance of two topologies is analyzed under inverter short-circuit fault. As highlighted in [4], short-circuit faults are the most constraining ones because of high peak-currents generated. A specific fault tolerant control has the purpose of reducing torque oscillation and, consequently, the peak-currents in degraded mode [6][7]. Because of this, two degraded modes with different hardware reconfigurations were included in this paper analysis.

Both topologies are open-winding and composed of two symmetrical six-phase machines. The first topology is a classical H-bridge drive (Fig. 3), while the second one presents a series connection between the machines (Fig. 4) where the number of transistors is halved. A decrease of the number of current sensors, transistors and, consequently, the number of drivers compared to a classical topology, allows a global cost and mass reduction. That is particularly true if the switch ratings do not increase drastically for the series connected machine topology. Besides, as the series-connection topology presents a higher value of inductive components in comparison with the H-bridges topology, currents harmonics amplitude, which may reach high values in degraded mode, are expected to be lower. On contrary, as currents cross both machines even if only one is driven, the copper losses raises and subsequently the global efficiency are expected to be lower.

Series connected machines in the 2nd topology will only be considered as a better solution if the global cost (investment cost and running cost) are lower than the concurrent topologies. Short time missions (e.g. thruster) may appear as an application in accord with the series connection topology, because the running cost tends to be negligible in comparison with the investment cost.

In series connection topology, an independent control of each machine requires a specific coupling. Some papers [8]-[11], demonstrate that the number of DoF (in this case, independent currents) has to be higher than twice the number of machines, in a case of a sinusoidal back electromotive force (Back-EMFs). Otherwise, a more complex control using supplementary DoF is required for the torque oscillation compensation [11].

The paper is organized as follows. Section II describes the TVC system. In section III, two topologies are proposed and analyzed. Section IV explains the two analyzed reconfiguration strategies. Section V specifies the simulation conditions and some results are given.

II. TVC SYSTEM

Thrust Vector Control (TVC) system controls the rocket trajectory using two actuators that will move the thruster. These actuators are placed 90° from each other, in order to almost decouple the rotation in two orthogonal axes. The thruster movement includes two variables: the inclination angle

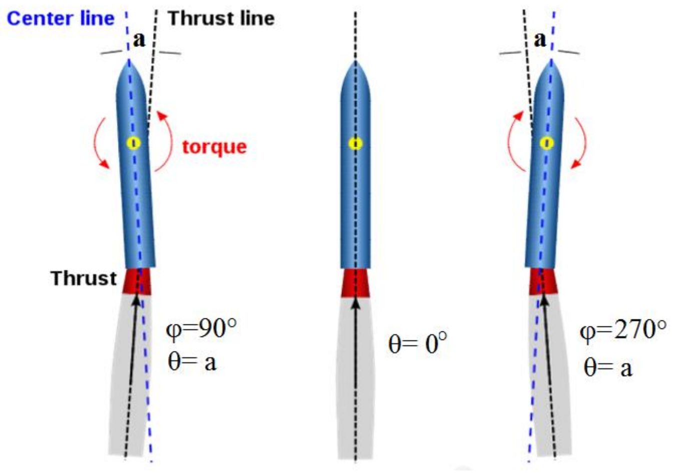

Fig. 1: Representation of the torque generation under 3 different thrust inclinations.

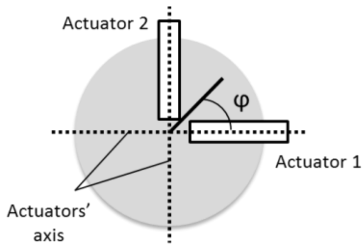

Fig. 2: Angle φ representation with actuators' axis as reference

between its axis and the rocket axis (θ – between 0° and 6°) and its direction (φ – between 0° and 360°), as shown in Fig. 1 and Fig. 2.

Because of the effort added of both actuators, equations (1) and (2) calculate the speed reference of each machine for a maximum inclination of the thruster (θ = 6°) in rad/s depending on the angle φ.

$$\Omega_{\mathrm{ref1}} = 100\ \cos(\varphi) \qquad (1)$$

$$\Omega_{\mathrm{ref2}} = 100\ \sin(\varphi) \qquad (2)$$

The TVC system profile of utilization is difficult to precise, because strong resistance forces applied in different directions, as the thrust has to ensure the imposed trajectory. Considering the duration of use, the thruster of the lower levels run during approximately 3 minutes, as the upper level run during some hours, depending of the rocket's mission.

III. Topologies

Both topologies analyzed in this study have two symmetrical six-phase open-end winding motors. In comparison to regular topologies with wye-coupling three-phase machines, the topologies proposed in this study are more adaptable to high-power and fault-tolerant applications. At first, a higher number of phases reduces the magnitude of current on each phase for the same power. Furthermore, the supplementary phases take the role of DoF assuring fault-tolerance of the system. Open-end windings improve fault-tolerance performance by adding one DoF in comparison to the wye-coupling machine and also by the independent supplying aspect [1][4]. However, those topologies need a high number of transistors (two inverter legs per phase).

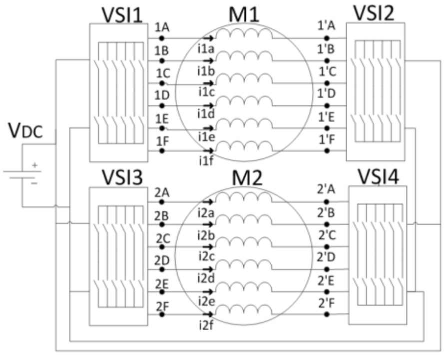

Fig. 3: The H-bridges topology

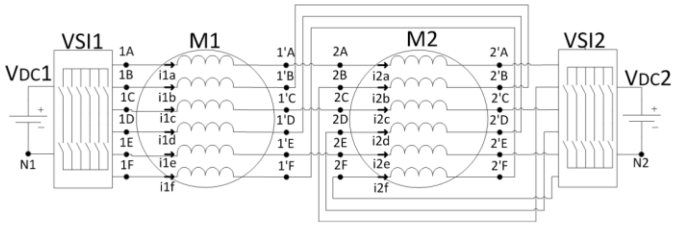

Fig. 4: The RIMM topology

The H-bridges topology (Fig. 3) is composed by two machines independently supplied. This topology can be already found in some naval and aeronautic applications. The control of this topology is simple, but needs a high number of switches (N_{sw}) (48 switches for 24 inverter legs).

The second topology analyzed in this paper is named RIMM (Redundant Inverter Multiple Machine) (Fig. 4). In the interest of halving the power electronic components, the machines are connected in series. Two DC-sources supply the topology, representing a redundancy of the source, but, at the same time, reducing one DoF. In this study, the voltage between the negative potential points of the sources (v_{n1n2}) is not controlled. However, this voltage can be controlled to increase the system performance in case of short-circuit inverter fault [7].

The independent speed and torque control of the machines is ensured by the innovative coupling between them.

$$[I_2] = [K][I_1] \qquad (3)$$

$$\begin{bmatrix} i_{2a} \\ i_{2b} \\ i_{2c} \\ i_{2d} \\ i_{2e} \\ i_{2f} \end{bmatrix} = \begin{bmatrix} 1 & 0 & 0 & 0 & 0 & 0 \\ 0 & -1 & 0 & 0 & 0 & 0 \\ 0 & 0 & 1 & 0 & 0 & 0 \\ 0 & 0 & 0 & -1 & 0 & 0 \\ 0 & 0 & 0 & 0 & 1 & 0 \\ 0 & 0 & 0 & 0 & 0 & -1 \end{bmatrix} \begin{bmatrix} i_{1a} \\ i_{1b} \\ i_{1c} \\ i_{1d} \\ i_{1e} \\ i_{1f} \end{bmatrix} \qquad (4)$$

Applying six-phase Concordia transformation ($[C_6]$) to equation (3), a symmetrical six-phase machine is decomposed into four decoupled fictitious machines [12]: two homopolar machines and two two-phase machines. Each fictitious machine interacts with some back-EMF harmonics to generate a torque, as shown in TABLE I.

TABLE I. HARMONIC EMF FOR EACH FICTITIOUS MACHINE

Six-phase machine	**First homopolar machine (h1)**	**Secondary homopolar machine (h2)**	**Main machine (mα mβ)**	**Secondary machine (sα sβ)**
Back-EMF harmonics	H0, H6, H12, …	H3, H9, …	H1, H5, H7, H11 …	H2, H4, H8, H10, …

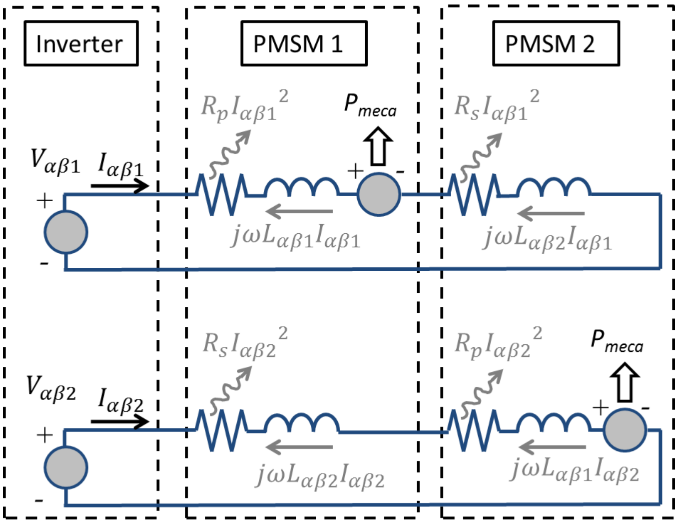

Fig. 5: Scheme showing the series connection between the fictitious machines.

The main machine is the one to be controlled to generate the highest torque with less current.

TABLE I shows that the first homopolar machine (h_1) and the secondary machine ($s\alpha$ $s\beta$) interact with even harmonics of the back-EMFs after the Concordia transformation. Even back-EMFs harmonics are null in regular electric machines because of morphologic aspects of winding symmetry. Anyway, Back-EMF of the analyzed model is sinusoidal; so the total average torque of the six-phase machines is generated by the main-machine.

$$\left[I_{1_{\alpha\beta}}\right] = [C_6][K]^{-1}[C_6]^T \left[I_{2_{\alpha\beta}}\right] \tag{5}$$

$$\left[I_{1_{\alpha\beta}}\right] = \begin{bmatrix} 0 & 1 & 0 & 0 & 0 & 0 \\ 1 & 0 & 0 & 0 & 0 & 0 \\ 0 & 0 & 0 & 0 & 1 & 0 \\ 0 & 0 & 0 & 0 & 0 & -1 \\ 0 & 0 & 1 & 0 & 0 & 0 \\ 0 & 0 & 0 & -1 & 0 & 0 \end{bmatrix} \left[I_{2_{\alpha\beta}}\right] \tag{6}$$

$$\begin{bmatrix} I_{h11} \\ I_{h21} \\ I_{m\alpha1} \\ I_{m\beta1} \\ I_{s\alpha1} \\ I_{s\beta1} \end{bmatrix} = \begin{bmatrix} I_{h12} \\ -I_{h22} \\ I_{s\alpha2} \\ -I_{s\beta2} \\ I_{m\alpha2} \\ -I_{m\beta2} \end{bmatrix} \tag{7}$$

$$\begin{bmatrix} I_{m\alpha1} \\ I_{m\beta1} \end{bmatrix} = \begin{bmatrix} I_{s\alpha2} \\ -I_{s\beta2} \end{bmatrix} \rightarrow [I_{m1}] = [I_{s2}]^* \tag{8}$$

$$\begin{bmatrix} I_{s\alpha1} \\ I_{s\beta1} \end{bmatrix} = \begin{bmatrix} I_{m\alpha2} \\ -I_{m\beta2} \end{bmatrix} \rightarrow [I_{s1}] = [I_{m2}]^* \tag{9}$$

Fig. 5 illustrates equations (8) and (9) representing the series connection of the fictitious machines, because they conduct the same currents. As mentioned above, two secondary machines do not generate torque, which can lead to a simple and independent control of M1 and M2 torque by controlling $I_{\alpha\beta1}$ and $I_{\alpha\beta2}$ respectively.

IV. Reconfiguration Modes

Two hardware reconfigurations are analyzed in this paper. This means that the control strategy (to generate the references of voltage) doesn't change, but some transistors will have their state (open or close) imposed.

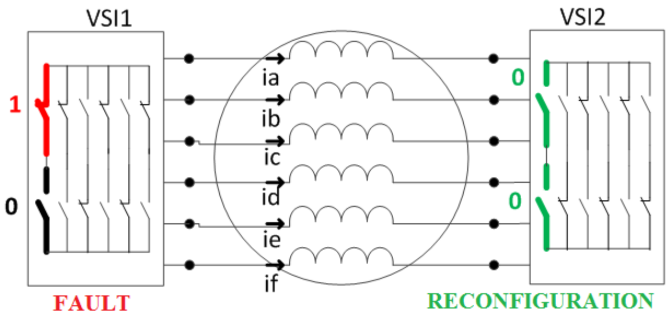

Fig. 6: Representation of the reconfiguration strategy 1.

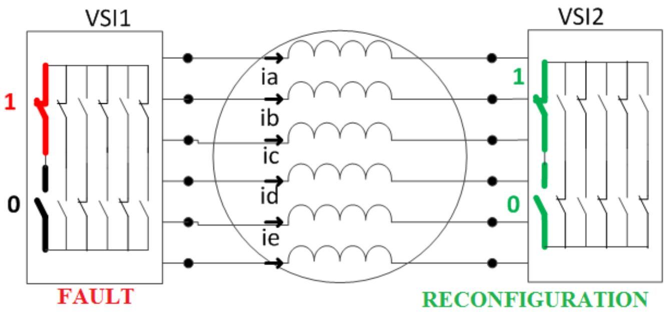

Fig. 7: Representation of the reconfiguration strategy 2.

Reconfiguration 1 opens all the switches of the corresponding leg. Fig. 6 gives an example where the top switch of the first leg of the VSI1 is short-circuited. The reconfiguration 1 is achieved by an opening of two transistors of the first leg of the VSI2. That doesn't mean that the current of the first phase will be null. A real switch can be represented by an ideal transistor connected with a diode in anti-parallel. So the diode will allow the current to flow in one direction.

Reconfiguration 2 will control the corresponding leg of the second inverter to reproduce the same short-circuit faulty leg as the VSI1 (Fig. 7). As a consequence, the phase (or the phases) supplied by the faulty legs will be connected to the same voltage in both sides. Similarly to the reconfiguration 1, the current of the faulty phase is not nullified but its value depends on the Back-EMF and the voltage v_{n1n2}.

In general, a reconfiguration needs a fault detection system that detects precisely and quickly the fault in order to activate the reconfiguration strategy. For the first reconfiguration strategy implementation, fault detection system has to identify the faulty phase, while the reconfiguration 2, needs information of the faulty switch and the faulty type (open-switch or short-circuit). Even so, the fault-detection strategies are not analyzed in this paper.

V. Simulation

A. Drive model

Machine's parameters are not similar for both topologies. Because of aerospace constraints, the DC-bus voltage is fixed, so the drive has to be adapted to it. The number of coil turns has been defined by taking into account the drive normal mode performance, impacting on the phase resistance, inductance and magnetic flux, as TABLE II shows.

TABLE II. MACHINE PARAMETERS

	H-bridges	**RIMM**
Coil turns	N	N*0.78
R_s	0.043Ω	0.026Ω
$L_{m\alpha\beta}$	0.455mH	0.277mH
$L_{s\alpha\beta}$	0.455mH	0.277mH
L_h	0.455mH	0.277mH
e_{q1}/Ω	0.32	0.25
Pole pairs number (p)	7	7

B. Speed reference

In the thruster pay-load, two kinds of speed references must be ensured by each topology. Both speed references represent a maximum inclination ($\theta = 6°$) of the thruster in comparison to the rocket axis. For each topology, the sizing of the inverter will be achieved by considering the worst case for the considered topology.

As H-bridges topology has the machines independently supplied, the highest peak-current will be generated when the displacement direction is $\varphi = 0°$ on one actuator axis and $\Omega_{ref} =$ 100 rad/s for the other actuator axis.

On other hand, as the two machines are in series, the most constraining speed reference for RIMM topology is when displacement at $\varphi = 45°$, with both machines running simultaneously at Ω_{ref}= 70.7 rad/s.

C. Faults simulation

For the short-circuit fault simulation, the top switch of the phase A of the inverter VSI1 in both topologies is short-circuited. To avoid a short-circuit of the DC-bus, the bottom switch of the same leg has to be 'open'.

For the reconfiguration 1 simulation, both switches of the phase A of the inverter VSI2 will be opened, similar to Fig. 6. In the reconfiguration 2, the top switch of the phase A of the inverter VSI2 will be closed, and the bottom switch of this same inverter leg will be opened, as Fig. 7.

D. Results and analysis

Fig.8 presents the simulation results for the two different topologies presented in section III under healthy and faulty modes at the most constraining speed reference.

Peak-currents (I_{pk}) are obviously higher in faulty mode than in healthy one because the currents in the healthy phases have to increase to reach the required speed and torque as before the fault, as shown in Fig. 9 to Fig. 13.

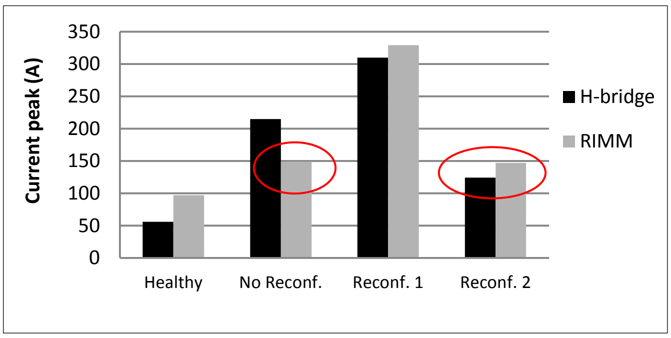

Fig.8: Peak currents obtained under normal mode and under short-circuit switch fault operations with two proposed topologies.

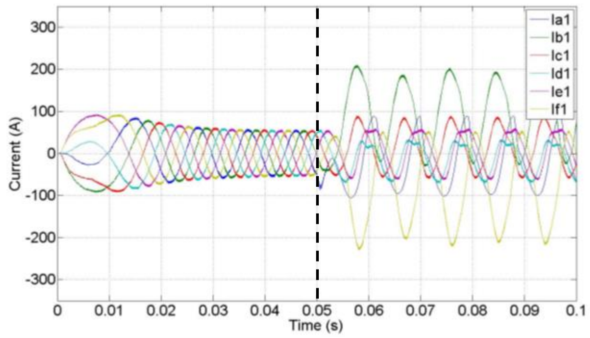

Fig. 9: H-bridge's currents without reconfiguration.

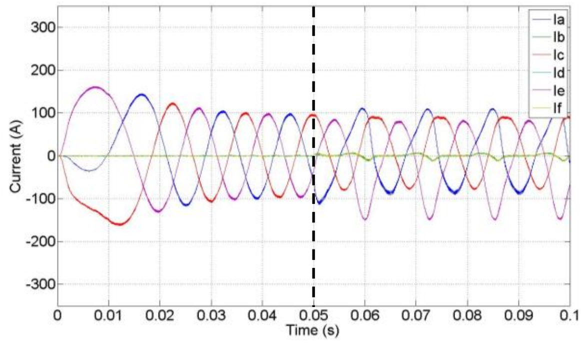

Fig. 10: RIMM's current without reconfiguration.

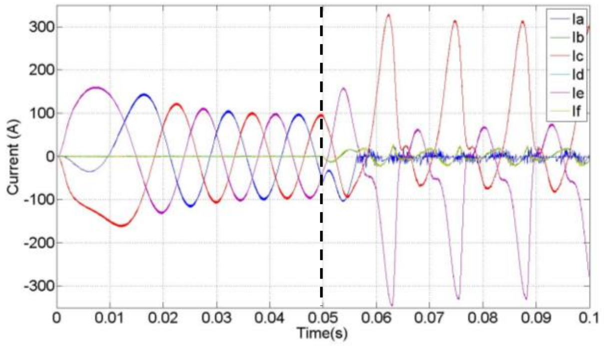

Fig. 11: RIMM's current with reconfiguration 1.

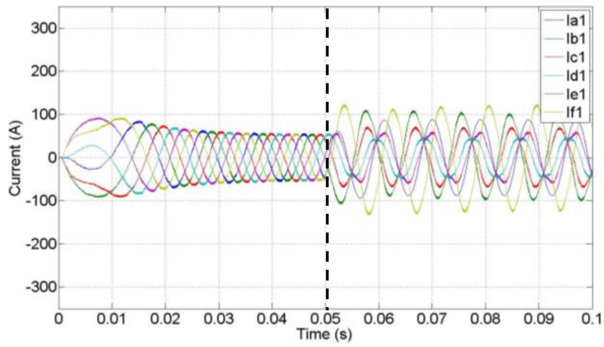

Fig. 12:H-bridge's current with reconfiguration 2.

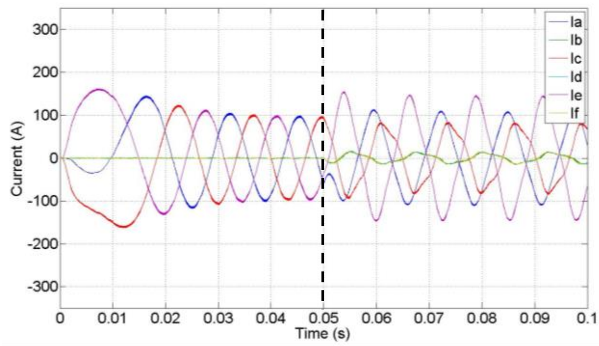

Fig. 13:RIMM's current with reconfiguration 2.

Fig. 9 and Fig. 10 give the obtained currents of each topology before and after a short-circuit switch fault without reconfiguration. High homopolar harmonics in H-bridge currents explain the higher peak-currents and current phases more unbalanced. On the other hand, the RIMM topology doesn't have a path for the even homopolar current harmonics.

Because of the special series connection, when both machines have exactly same running conditions (speed reference, resistance force and initial rotor position) three of six current phases tend toward zero, consequently, the peak of those currents are high.

By observing Fig. 8, the reconfiguration 1 has the highest peak-currents for both topologies in both speed references in comparison with all the other modes.

Differently than the reconfiguration 1, the second reconfiguration strategy reduces the peak-currents of both topologies, comparing to the no reconfiguration degraded mode. Otherwise, the graphic shows a higher impact of the reconfiguration for the H-bridges topology than for the RIMM topology, a reduction of almost 100A in the peak-current for the H-bridges topology while RIMM's peak-current stays almost unchanged (about 150A). The reduction of the homopolar currents explains these results. Without reconfiguration, the RIMM topology conducts low homopolar currents because of the two isolated source neutral points.

Beside of it, the reconfiguration 2 is less adaptable to the RIMM topology because the current conducted by the faulty leg is generated by the Back-EMF plus the voltage v_{n1n2}.

For a general comparison, the minimum value of peak-current is obtained in reconfiguration 2 with the H-bridges topology (around 125A), 16% lower than RIMM's peak current at the same reconfiguration, but with twice more switches. The global apparent power (in VA) (S_{gl}) of the "H-bridges" topology is in this case roughly 168% higher than with the RIMM topology, as calculated by equations (10) and (11) and shown in Fig. 14.

$$S_{sw} = V_{DC} * I_{pk} \tag{10}$$

$$S_{gl} = N_{sw} * S_{sw} \tag{11}$$

Furthermore, RIMM topology does not need reconfiguration strategies to reduce significantly its required investments, being exempt of reconfiguration operational constraints. On the other hand, H-bridges' global apparent power is almost three times higher without reconfiguration (Fig. 14).

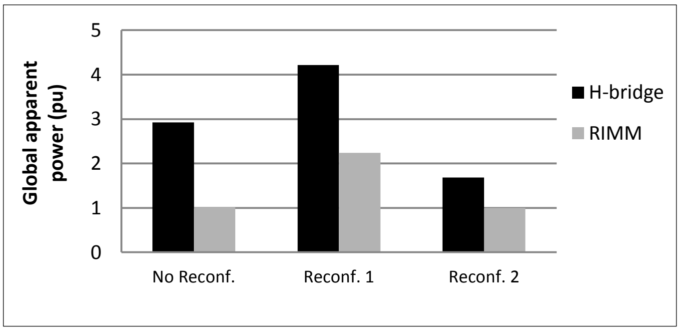

Fig. 14: Comparison of the global power of the switches set (lower value being taken as reference).

VI. CONCLUSION

This paper compares two topologies comprising each one inverter legs and two symmetrical six-phase machines. The comparison criterion is the global sizing of the inverter, so the global apparent power. The RIMM topology needs 12 inverter legs in comparison with the 24 inverter legs of the H-bridges topology. As the voltage constraint, due to identical DC-voltage source, is the same for the two topologies, it is the peak current which is the determining factor for the transistor's apparent power.

As the short-circuit inverter switch induces on the peak current a more severe constraint than the normal mode operation, the comparison is done in this case, considering then three different strategies of control.

The RIMM topology shows a better performance in term of power electronic components and power rate of inverters, for the two best available strategies in case of inverter switch short-circuit fault. Even if the H-bridge peak-currents for reconfiguration 2 were the lowest peak-currents obtained, RIMM's global apparent power is lower without reconfiguration or with reconfiguration 2.

REFERENCES

[1] J. Bennett , G. Atkinson , B. Mecrow and D. Atkinson "Fault tolerant design considerations and control strategies for aerospace drives", *IEEE Trans. Ind. Electron.*, vol. 59, no. 5, pp.2049 -2058 2011

[2] M. Villani , M. Tursini , G. Fabri and L. Castellini "High reliability permanent magnet brushless motor drive for aircraft application", *IEEE Trans. Ind. Electron.*, vol. 59, no. 5, pp.2073 -2081 2012

[3] L. de Lillo , L. Empringham , P. Wheeler , S. Khwan-On , C. Gerada , M. Othman and X. Huang "Multiphase power converter drive for fault-tolerant machine development in aerospace applications", *IEEE Trans. Ind. Electron.*, vol. 57, no. 2, pp.575 -583 2010

[4] B. A. Welchko, T. A. Lipo, T. M. Jahns, and S. E. Schulz, "Fault tolerant three-phase AC motor drive topologies: A comparison of features, costs, and limitations," *IEEE Trans. Power Electron.*, vol. 19, no. 4, pp. 1108-1116, July 2004.

[5] R. R. Errabelli and P. Mutschler, "Fault-Tolerant Voltage Source Inverter for Permanent Magnet Drives," *IEEE Transactions on Power Electronics*, vol. 27, no. 2, pp. 500–508, Feb. 2012.

[6] A. Mohammadpour, S. Mishra, and L. Parsa, "Fault-Tolerant Operation of Multiphase Permanent-Magnet Machines Using Iterative Learning Control," *IEEE Journal of Emerging and Selected Topics in Power Electronics*, vol. 2, no. 2, pp. 201–211, Jun. 2014.

[7] N. K. Nguyen, F. Meinguet, E. Semail, and X. Kestelyn, "Fault-Tolerant Operation of an Open-End Winding Five-Phase PMSM Drive with Short-Circuit Inverter Fault," *IEEE Transactions on Industrial Electronics*, pp. 1–1, 2015.

[8] E. Levi, M. Jones, S.N. Vukosavic, H.A. Toliyat, "A Novel Concept of a Multiphase, Multimotor Vector Controlled Drive System Supplied From a Single Voltage Source Inverter", *IEEE Transactions on Power Electronics*, vol. 19, no. 2, March 2004, pp. 320-335.

[9] D. Dujic, M. Jones, E. Levi, and O. Lopez, "DC-bus utilisation in series-connected multi-phase machines supplied from a VSI with a composite phase number," *Electrical Machines (ICEM), 2010 XIX International Conference*, Rome, 2010, pp. 1–6.

[10] A. Iqbal , S. Vukosavic , E. Levi , M. Jones and H. A. Toliyat "Dynamics of a series-connected two-motor five-phase drive system with a single-inverter supply", *Conf. Rec. IEEE IAS Annu. Meeting*, pp.1081 -1088 2005

[11] E. Semail, E. Levi, A. Bouscayrol, and X. Kestelyn, "Multi-machine modelling of two series connected 5 phase synchronous machines: effect of harmonics on control," Power *Electronics and Applications, 2005 European Conference*, Dresden (Germany), Sept. 2005, pp. 1-10

[12] X. Kestelyn, E. Semail, "A Vectorial Approach for Generation of Optimal Current References for Multiphase Permanent Magnet Synchronous Machines in Real-time", *IEEE Transactions on Industrial Electronics*, Vol 58, N°11, pp5057-5065, Nov 2011.